J Math Model Algor (2009) 8:363–385
DOI 10.1007/s10852-009-9112-6

Some Observations on the TLM Numerical Solution of the Laplace Equation

D. de Cogan · X. Gui · M. Rak

Received: 26 October 2008 / Accepted: 20 May 2009 / Published online: 11 June 2009

Abstract This paper describes progress on the TLM modelling of the Laplace equation, in particular, how the rate of convergence is influenced by the choice of scattering parameter for a particular discretisation. The hypothesis that optimum convergence is achieved when the real and imaginary parts for the lowest harmonic in a Fourier solution cancel appears to be upheld. The Fourier solution for the problem has been advanced by a better understanding of the nature of the initial excitation. The relationship between the form of the initial condition used in this and many other numerical solutions of the Laplace equation and oscillatory behavior in the results is given a firmer theoretical basis. A correlation between TLM numerical results and those obtained from matrix spectral radius calculations has confirmed much previous work.

Keywords Transmission line matrix (TLM) method · Differential equations · Laplace equation · Spectral radius · Fourier solutions

Mathematics Subject Classifications (2000) 35J99 · 35P99 · 65M06 · 65M30

D. de Cogan (✉)
School of Computing Sciences, University of East Anglia,
Norwich NR4 7TJ, UK
e-mail: ddc@uea.ac.uk

X. Gui
NXT Energy Solutions Inc., Suite 1400, 505-3rd Street SW,
Calgary, Alberta T2P 3E6, Canada

M. Rak
Institute of Physics, Technical University of Łódź,
ul. Wolczanska 219, PL-93-005 Łódź, Poland

1 Introduction

There are a wide variety of numerical techniques for the solution of the Laplace equation in different dimensions. These range from probabilistic to finite difference approaches. Amongst the first practical approaches for numerically solving partial differential equations was Southwell's relaxation method, originally devised for "solving stresses in highly redundant pin-jointed frameworks—a means which obviates the necessity of solving large numbers of simultaneous equations" [1]. Dusinberre's approach to heat-flow was even closer to what we might now recognise as finite difference techniques [2]. His observation, that in a model space bounded by a surface at T_{hot} the initial excitation must be $T_{\text{hot}}/2$ in order to avoid strong oscillatory behaviour in the results, is of particular relevance in this paper. Convergence has been characterised by authors such as Ames [3] and Morton and Mayers [4] and the relative performance of Jacobi and Gauss–Seidel schemes are well known.

The use of electrical network analogue models is a well established approach to solving partial differential equations (PDEs). Within this array of approaches, Transmission Line Matrix (TLM) is a relative newcomer. In this method an electrical network whose behaviour closely mimics the physical problem is constructed. This is based mainly on a network (a mesh or matrix) of 'transmission lines'. The behaviour of transmission lines is well understood and fully described in electromagnetic theory. Their most important property in this context is the introduction of a time-delay for signals travelling between points in the electrical network. The distribution of mesh points in the modelled space provides the spatial discretisation of the problem while the time delays in the transmission lines provides the temporal discretisation. A time-discrete train of current or voltage impulses is injected into the network to simulate the physical excitation (heat, temperature, initial material flux etc.) and solution of the TL network analogue is then achieved by the repeated application of a relatively simple set of rules. Thus TLM can be considered as a form of cellular automaton modelling, where the transition rules are determined by the laws of electromagnetics. TLM has been used extensively in the modelling of electromagnetic [5] and diffusion [6] phenomena. It has been used in a phenomenological way to model chromatography [7] as well as minority carrier decay in solid-state physics [8]. It has also been shown to provide a continuum of solutions between macro-scale and micro-scale diffusion [9].

Johns, the pioneer of TLM, described a specific formulation as a "simple, explicit and unconditionally stable" method for solving the diffusion equation [10]. He discussed the relationship between this and various forms of finite difference formulations in terms of a technique called *Propagation Analysis*. The treatment is virtually inaccessible for all except those well versed in electromagnetic theory, but a simple presentation is now available [11].

Johns, in a private discussion with one of the authors (DdeC) observed that it should be possible to use TLM to solve the Laplace equation "once the transients have passed through the time derivatives will eventually tend towards zero". This was confirmed and, while investigating the influence of choice of operational parameters, conditions that led to an accelerated convergence were observed [12]. An explanation for this phenomenon based on the diffusion equation is not possible. However [13] has shown that it can be explained if one uses the Telegraphers' equation.

The physical problem which is modelled using TLM was treated analytically using Fourier methods. The solution was not pursued to completion because of some uncertainty about the way in which TLM treats the initial conditions. Indeed, there seems to have been very little questioning of the basis for the observation by Dusinberre [2] that the *initial* excitation must be $T_{\text{hot}}/2$ for thermal problems (or $V_{\max}/2$ for potential problems) in order to avoid strong oscillatory behaviour in the results.

The results which are cited for the accelerated convergence of TLM solutions of the Laplace equation have a mirror in the 'successive over-relaxation' (SOR) finite difference method [14]. In this case analytical solutions are available which account for behaviour of $\Re[M]$, the spectral radius[1] of the underlying matrix as a function of the acceleration factor ω. However the shape of the $\Re[M(\omega)]$ plot for a given discretisation appears to be quite different from what we observe using our convergence criteria. Indeed, when we use these criteria on either SOR or TLM we observe fine structure (ripples), which are not accounted for by simple theory.

Finally, our previous work in this area identified a small discrepancy between the optimum convergence, as predicted by Fourier analysis and what was observed in TLM numerical experiments. We believe that we now have the answer to this and to the several other questions which have been raised above.

This paper will start with a brief introduction to the TLM algorithm for modelling the Laplace equation. We highlight the reflection coefficient which contains information on the physical properties and the space and time discretisations. This is the key element in the technique of *mesh scaling* which provides insight into the nature of the initial excitation. At this point we are able to proceed with a full Fourier treatment of the physical problem as modelled by TLM. The remainder of the paper will then address the various issues which have been raised earlier.

2 TLM Schemes for the Solution of the Laplace Equation

The TLM numerical method has its foundations in electromagnetic theory and extensive details may be found in [15].

The fundamental component in TLM is the transmission line which has distributed electrical parameters: C_{d}, the capacitance per unit length, and L_{d}, the inductance per unit length. Signals imposed on transmission lines experience a time delay which is enforced by the velocity, which is given by:

$$v = \frac{1}{\sqrt{L_{\text{d}} C_{\text{d}}}}. \tag{1a}$$

The ratio of the electrical parameters is the basis for the impedance, which is given by:

$$Z = \sqrt{\frac{L_{\text{d}}}{C_{\text{d}}}} = \sqrt{\frac{L}{C}} \ \left(\text{independent of length}\right). \tag{1b}$$

[1]The symbol, 'ρ' is normally used to denote spectral radius, but as it is also used extensively to denote reflection coefficient in TLM, 'ℜ' has been used here.

From these we can get a measure of the time delay experienced by a signal on a line:

$$\Delta t = Z\, C_{\mathrm{d}} \Delta x \quad \text{or} \quad Z = \frac{\Delta t}{C} \tag{2a}$$

and

$$\Delta t = \frac{L_{\mathrm{d}} \Delta x}{Z} \quad \text{or} \quad Z = \frac{L}{\Delta t}. \tag{2b}$$

These are strictly true for conditions where the signal frequency tends towards zero, but they can still be used for low frequencies. They constitute about the only basic approximation that is used in the TLM method.

So long as the impedance of a transmission line is uniform then signals in transit suffer no perturbation. However, if the impedance changes at some location, then there will be reflections and transmissions. When an impulsive signal travelling on a line of impedance Z encounters a change of line impedance to Z_B, part of the signal will be reflected and part will be transmitted. The reflection coefficient is:

$$\rho = \frac{Z_B - Z}{Z_B + Z}. \tag{3}$$

In TLM models for diffusion we add resistance to the line, so that our basic network is composed of a series connection: transmission-line/resistor/resistor/transmission-line etc. Thus the non-matching impedance in Eq. 3 comprises two resistors, each of value, R and a terminating impedance of value $Z\,(Z_B = 2R + Z)$. In this case we would have a reflection coefficient:

$$\rho = \frac{R}{R + Z}. \tag{4}$$

The transmission coefficient $\tau = 1 - \rho$.

The exact scheme by which we account for the scattering of impulse analogues depends on the point at which we choose to make our observations. We could monitor the passage of impulses from a point which is located half-way along a transmission line. In this formulation each node comprises a length, Δx of line with a resistor at each end which links to an identical arrangement at neighbouring nodes. The alternative approach is to centre the observer between two resistors and place half-lengths of line on either side which link to adjacent nodes (see Fig. 1). The results from both of these are equivalent. The link-line node, which will be used here displays one curiosity, namely 'jumps-to-zero', but these are easily accommodated.

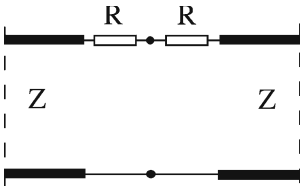

Fig. 1 A single 'link-line' node as used in TLM. The centre, at which observations are made at discrete time intervals, Δt, is surrounded by two resistors. These are connected to two transmission (delay) lines, each of discrete length, $\Delta x/2$

In common with most works on the subject we will use a voltage-based analysis. At time[2] $m\Delta t$ two incident pulses, ${}_m^iV_L(x)$ and ${}_m^iV_R(x)$ are travelling along transmission lines and approaching the resistors in Fig. 1 from left and right respectively. The Thévenin equivalent circuit assumes that these pulses have originated from voltage sources $2\,{}_m^iV_L(x)$ and $2\,{}_m^iV_R(x)$, and we can use a simple potential divider formula to calculate the contribution from each to the voltage at the centre of the node at iteration, m:

$$ {}_mV(x) = 2\,{}_m^iV_L(x)\,\frac{(R+Z)}{(2R+2Z)} + 2\,{}_m^iV_R(x)\,\frac{(R+Z)}{(2R+2Z)} = {}_m^iV_L + {}_m^iV_R. \tag{5} $$

The scattering of these incident pulses (reflection and transmission) is described by:

$$ \begin{aligned} {}_m^sV_L &= \rho\,{}_m^iV_L + \tau\,{}_m^iV_R, \\ {}_m^sV_R &= \tau\,{}_m^iV_L + \rho\,{}_m^iV_R. \end{aligned} \tag{6} $$

This is the *Scattering Rule* in the TLM algorithm.

Each of the scattered pulses now takes a time $\Delta t/2$ to travel to the boundaries of the node and a further time, $\Delta t/2$ before becoming incident pulses at adjacent nodes. In the simplest analysis we then predict what is incident at node (x), based upon what was scattered from nodes $(x+1)$ and $(x-1)$:

$$ \begin{aligned} {}_{m+1}^iV_L(x) &= {}_m^sV_R(x-1), \\ {}_{m+1}^iV_R(x) &= {}_m^sV_L(x+1). \end{aligned} \tag{7} $$

This is the *Incidence Rule* in the TLM algorithm.

A TLM scheme comprises the repeated application of theses two rules for every node in our space. Time advances by Δt every time we repeat this automaton. We can, at any time, $m\Delta t$, inspect the potential at each node by using Eq. 5.

In a TLM routine for one-dimensional heat-flow in a rod we start with the length and the time for which the simulation is to be run. After a choice of spatial and temporal discretisations we can write $L = M\Delta x$ and $t = m\Delta t$. The nodal volume together with the cross-sectional area are used in conjunction with the material parameters of density, specific heat and thermal conductivity to give meaning to the components of Eq. 4, which we rewrite the reflection coefficient as:

$$ \rho = \frac{1}{1 + Z/R} \tag{8} $$

and since $Z = \dfrac{\Delta t}{C}$ we have:

$$ \rho = \frac{1}{\left[1 + \frac{\Delta t}{RC}\right]}. \tag{9a} $$

The product RC has units [time]. $RC = R_{\mathrm{d}}C_{\mathrm{d}}\Delta x^2$ where the subscripts represent distributed resistance and capacitance.

[2]The convention amongst TLM modellers is to use 'k' for the time index. The letter 'm' is used here to avoid confusion as 'k' is already used in Fourier solutions.

The product $R_d C_d$ has units [time] [distance]$^{-2}$ which identical to the units for the diffusion coefficient, D. Thus we can re-write Eq. 9a in terms of D and the spatial and temporal discretisations:

$$\rho = \frac{1}{\left[1 + D\frac{2\Delta t}{\Delta x^2}\right]}. \tag{9b}$$

Pulses within the computational space will interact with boundaries and these are described as follows. If the 'high' value boundary located at $x = 0$ is fixed at a potential of 100 V then an impulse scattered to the left at node $x = 1$ travels a distance $\Delta x/2$ where it encounters the 100 V boundary. The impulse that is returned to the centre of node (1) at the end of one iteration time-step (Δt) is given by:

$$_{m+1}^{i}V_L\,(1) = 100 - {}_{m}^{s}V_L\,(1)\,. \tag{10}$$

By similar argument the impulse reflected at the 'low' boundary ($V = 0$), located beyond node (M) on the right side of the problems is given by:

$$_{m+1}^{i}V_R\,(M) = 0 - {}_{m}^{s}V_R\,(M)\,. \tag{11}$$

The local potential at any iteration can be obtained by the superposition of pulses from left and right as per Eq. 5.

If the TLM scheme described above is run for large values of iteration time, m, then the transients die away and the ultimate solution is a solution of the Laplace equation. We see that Δt appears in Eq. 8 and yet it has no meaning in the Laplace equation. Previous work [12] demonstrated that there was an optimum choice of reflection coefficient which was dependent on the discretisation ($M = L/\Delta x$) that was used. Simulations using this value converged extremely rapidly. This effect can be explained using a Fourier-based solution of the associated telegraphers' equation [13]. The associated analysis predicts that the lowest Fourier component can be inhibited when $\tau/\rho = M/\pi$. The agreement with TLM-based numerical experiments is good, but there is a small discrepancy which has prompted further work which is described here.

3 An Analysis of Constant-Voltage Initial Condition in the TLM Scheme

Any formal analysis of the TLM scheme that is used to solve the Laplace equation might immediately identify that the problem appears to be ill-posed. There are clearly a set of boundary conditions, but there is no indication of a proper initial condition. This was one of the reasons why the Fourier solution was not pursued to completion in previous work [13]. This apparent lack of discipline is not unique

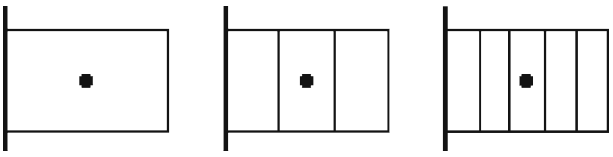

Fig. 2 A single TLM node (shown *left*) is scaled by factors three and then five in both space and time. We continue to monitor the same point of inspection at the same absolute time

Table 1 Potentials as a function of mesh scaling

S	$V(x_0)$									
1	50.00									
3	87.50		65.63		28.13					
5	92.8		79.48		65.59		53.05		24.11	
7	94.97		85.39		75.49		66.21		56.79		48.09		22.44
9	96.13		88.66		80.99		73.66		66.21		59.17		52.08		45.44		21.52
11	96.85		90.74		84.48		78.44		72.31		66.42		60.48		54.83		49.16		43.79		20.95

Centre is identified by heavy boundaries

to TLM. Finite difference schemes in their various forms seem to be equally guilty. It was noted at an early stage that non-oscillatory convergence is only obtained if an initial injection of $V_{\max}/2$ is used [2], something that has also been observed in TLM. In this section we start by using the technique of *mesh scaling* to investigate this 'rule-of-thumb' observation and to demonstrate that it is indeed a valid initial condition.

Let us start with a single node of length Δx situated next to a boundary which is held at 100 V. The initial injection at the boundary leads to an observation of 50 V at the node centre. However, the choice of discretisation is somewhat arbitrary, so that we could scale the mesh, so that $\Delta x \to \Delta x/2$ and $\Delta t \to \Delta t/2$. The propagation velocity would remain unchanged and if we were to examine the exact same position after $2\Delta t$ (in the new space–time regime) then we should be looking at the exact same thing. To simplify matters we choose a material with diffusion coefficient, D and discretisations, Δx, Δt arranged so that the initial value of reflection coefficient in Eqs. 9a and 9b is 1/2 when the scaling factor, $S = 1$. We then scale by *odd* numbers so that the original observation position always remains at the centre of a node (see Fig. 2).

The reflection coefficients for $S = 3$ and $S = 5$ are 1/4 and 1/6 respectively. In the first case we have an initial input of 50. In the second case we have an initial input of 50 at the node next to the boundary, but we do not sample our point of interest until we have done three iterations. In the case of a five-times scaling, we do not sample until after five iterations. The results up to $S = 11$ are shown in Table 1. The first thing is that scaling seems to move the $V_{\max}/2$ initial excitation closer to the boundary and further away from the point of interest.[3] What is now much more obvious than before is the apparent problem with the boundary on the cold side. In effect, the 'ill-defined' boundary is moving progressively from the hot junction to the cold junction.

[3]Note how the potential at the centre of the node seems to be tending towards a limit. $V(x_0)_{S=101} = 66.799$, $V(x_0)_{S=1,001} = 66.844$, $V(x_0)_{S=10,001} = 66.849$.

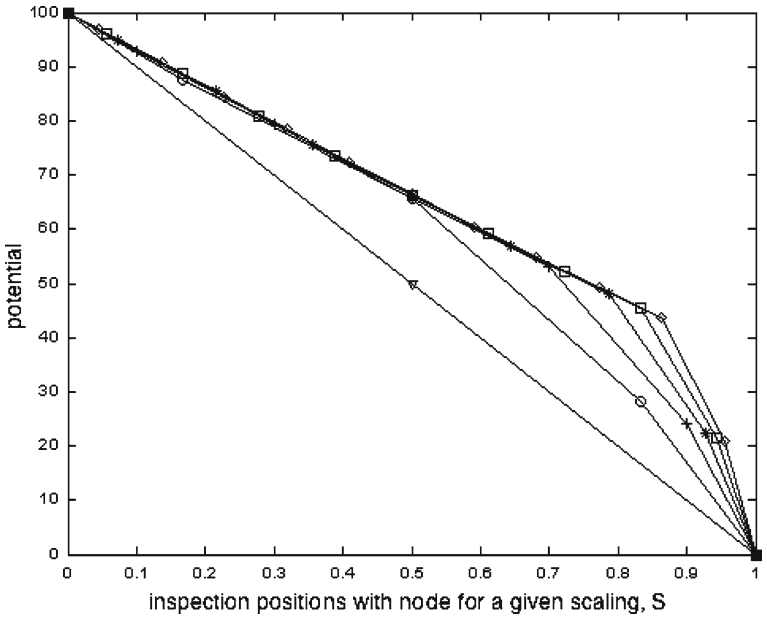

Fig. 3 Graphical representation of the data shown in Table 1. *Inverted triangle* $S = 1$, *open circle* $S = 3$, *plus sign* $S = 5$, *asterisk* $S = 7$, *open square* $S = 9$, *open diamond* $S = 11$

Some of these results are plotted in Fig. 3 and will be subject of further comment in the closing sections of the paper.

We now proceed to the second step, at $S = 1$, where we have to consider what is happening to two nodes in the simulation. When these are scaled we have a total of six nodes at $S = 3$ (see Fig. 4) and ten nodes at $S = 5$. When the simulation is run for $S = 3$ we wait until six iterations have been completed before inspecting the values at the centres of nodes 2 and 5. We could prepare a table as we have for $k = 1$, but we have simply plotted the resultant data in Fig. 5 and we can see that the values at the points of observation do not vary significantly except on the right where the boundary has not been defined. Indeed, this situation will persist until the propagating signal has hit $x = L$. By extension of this argument we conclude that we can by a process of progressive scaling move the first node in the simulation out of the bulk of the material and as close as we choose to the high boundary. In the limit as $\Delta x \to 0$, this $V_{\max}/2$ excitation is *at* the boundary where we have an initial gradient, $(\mathrm{d}V/\mathrm{d}x)_{m=0}$ is equal to 100.

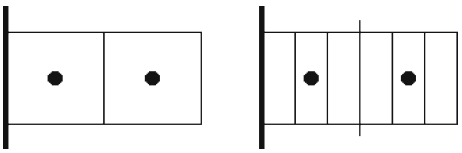

Fig. 4 The diagram on the *right* shows the two nodes (at scales $S = 1$ and $S = 3$) nearest the 100 V boundary that must be considered in a TLM simulation at $m = 2$

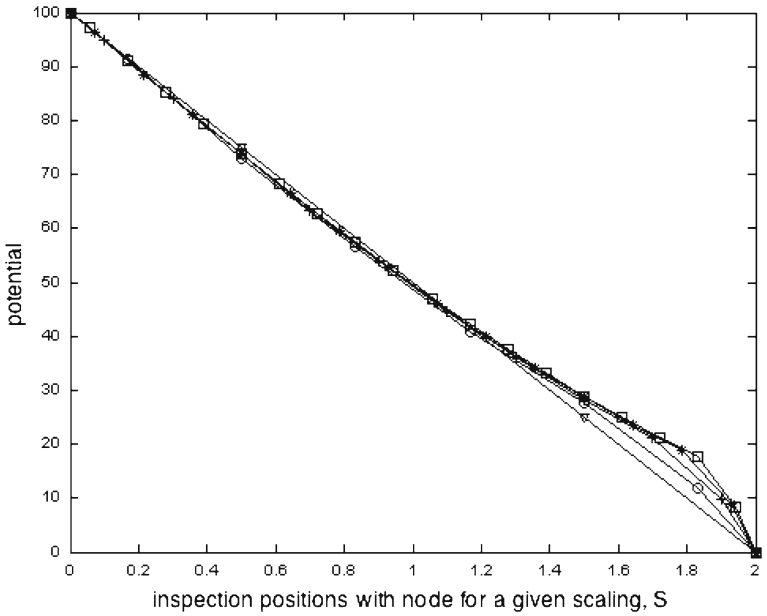

Fig. 5 The points shown as *inverted triangles* represent the potentials at nodes 1 and 2 at time $m = 2$ for $S = 1$. The other points represent the equivalent results when space and time are scaled (*open circle* $S = 3$, *plus sign* $S = 5$, *asterisk* $S = 7$, *open square* $S = 9$)

Gui and de Cogan [16] investigated TLM representations of boundary conditions, but in common with many other authors, have not discussed the situation at $t = 0$ in great detail. At the instant before we start the simulation we have a situation as shown in Fig. 6. Owing to the nature of transmission lines the rest of the circuit appears as a perfect absorber (a ground) so that we can concentrate on the charging

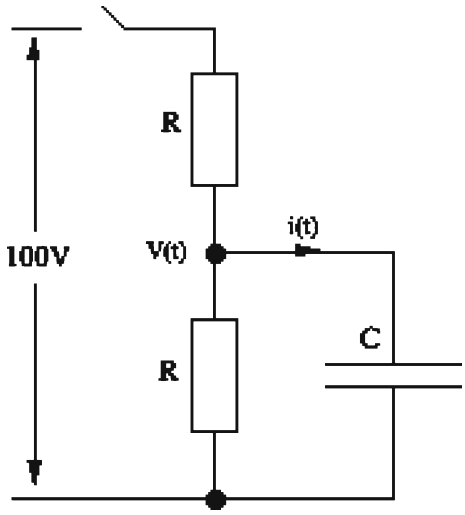

Fig. 6 The equivalent electric circuit which is observed from the viewpoint of the source at the instant at which it is switched on

up of the capacitor. Once the switch is closed the time dependence of the voltage *at the node centre* is given by:

$$V(t) = \frac{100}{2}\left[1 - e^{-\frac{2t}{RC}}\right]. \tag{12}$$

But, as we have already shown using our mesh-scaling argument, we can bring the node as close to the boundary as we like. We can make R and C as small as we like so that at the instant, $t = 0$ we have $V(\text{surface}) = 100/2$, which accounts for the observation of Dusinberre [2].

The rate of change of $V(t)$ can now be determined from Eq. 12:

$$\frac{\mathrm{d}V(t)}{\mathrm{d}t} = \frac{100}{RC}e^{-\frac{2t}{RC}}. \tag{13}$$

And from this we can obtain the time dependence of the current which charges the capacitance:

$$i(t) = C\frac{\mathrm{d}V(t)}{\mathrm{d}t} = \frac{100}{R}e^{-\frac{2t}{RC}}. \tag{14}$$

So, finally, we have the initial flux which we can use in our Fourier analysis:

$$i(t = 0) = \frac{100}{R}. \tag{15}$$

This completes the specification of the initial and boundary conditions.

4 A Fourier Treatment of the TLM Scheme for the Solution of the Laplace Equation

The Fourier solution for diffusion or lossy wave equations that are cited in most textbooks do not appear to be relevant to this particular problem because they are subject to boundary conditions of the form $V(x = 0, t > 0) = 0$, $V(x = L, t > 0) = 0$ with an initial condition $V(0 < x < L, t = 0) = f(x)$. We are interested in an inhomogeneous problem where we have $V(x = 0, t \geq 0) = 100$, $V(x = L, \geq 0) = 0$ and $V(0 < x < L, t = 0) = f(x)$. This problem can be overcome by defining a function $W(x, t) = 100(L - x)/L$ such that:

$$V(x, t) = U(x, t) + W(x, t). \tag{16}$$

U obeys the same PDE as V, but is subject to the homogeneous boundary conditions $U(0, t) = 0$, $U(L, t) = 0$, which can be treated using textbook methods.

Let us assume that we are solving:

$$\frac{1}{v^2}\frac{\partial^2 U}{\partial t^2} + \frac{1}{D}\frac{\partial U}{\partial t} = \frac{\partial^2 U}{\partial x^2} \tag{17}$$

(where v is velocity and D is diffusion constant).

We can separate variables by writing $U(x, t) = F(x)G(t)$. The second spatial derivatives of U can be represented as $F''G$, while the first and second time derivatives can be represented as $F\dot{G}$ and $F\ddot{G}$ respectively. We can then rewrite Eq. 17 as:

$$\ddot{G}F + \left(\frac{v^2}{D}\right)\dot{G}F = v^2 GF'' \tag{18a}$$

or

$$\frac{\ddot{G} + \left(\frac{v^2}{D}\right)\dot{G}}{v^2 G} = \frac{F''}{F}. \tag{18b}$$

The only non-trivial solution for the spatial (right) side of Eq. 18b is:

$$\frac{F''}{F} = -k^2. \tag{19}$$

So the left (temporal) side of Eq. 18b reduces to:

$$\ddot{G} + \left(\frac{v^2}{D}\right)\dot{G} + k^2 v^2 G = 0 \tag{20}$$

which has a solution:

$$G(t) = \exp\left[-\frac{At}{2}\right]\left[C_1 \exp\left[\frac{\sqrt{A^2 - 4B^2}}{2}t\right] + C_2 \exp\left[\frac{-\sqrt{A^2 - 4B^2}}{2}t\right]\right] \tag{21}$$

where $A = \frac{v^2}{D}$ and $B = kv$.

In proceeding further we must remember that since Eq. 19 is harmonic, k can take arbitrary integer values, so we can better write k_n and B_n. We can also represent the radical in Eq. 21 by $\beta_n = \sqrt{4B_n^2 - A^2}/2$ and reverting to Eq. 16 we have a Fourier solution:

$$V(x,t) = 100\left[\frac{L-x}{L}\right] + 100e^{-\frac{At}{2}} \sum_{n=1}^{\infty}\left[C_n \cos\beta_n t + C_n^* \sin\beta_n t\right]\sin(k_n x) \tag{22}$$

whose coefficients must now be determined, remembering that the first term on the right represents the convergent solution of the Laplace equation, while the summation term represents the error transient.

We start with the exponential and re-present it in TLM terminology. We know that $A = v^2/D$, so that we have:

$$\frac{At}{2} = \frac{v^2}{2D}t = \frac{1}{2}\frac{\Delta x^2}{\Delta t^2}\frac{2\Delta t\boldsymbol{\rho}}{\Delta x^2\boldsymbol{\tau}}m\Delta t = \frac{\boldsymbol{\rho}}{\boldsymbol{\tau}}m. \tag{23}$$

So, the linear relationship between the logarithm of the global error and the iteration index, m which was reported in [13] should be no surprise. Note that in the above we have set $v = \Delta x/\Delta t$. We will revisit this assumption later.

Returning to the error term in Eq. 22, we know that at $t = 0$ we have $U(L,0) = 0$, which implies that $C_n = 0$ and leaves us with:

$$V(x,t) = 100\left[\frac{L-x}{L}\right] + 100e^{-\frac{At}{2}} \sum_{n=1}^{\infty} C_n^* \sin(\beta_n t)\sin(k_n x). \tag{24}$$

The time derivative of this if taken at $t = 0$ yields:

$$\sum_{n=1}^{\infty} \beta_n C_n^* \cos(\beta_n t)\sin(k_n x) = g(x). \tag{25}$$

So, we arrive at the expression of C_n^*:

$$C_n^* = \frac{2}{L\beta_n} \int_0^L g(x) \sin\left(\frac{n\pi x}{L}\right) \mathrm{dx}. \tag{26}$$

We use Eq. 13 to give us the time derivative at $t = 0$ which is $g(x) = \frac{100}{RC}$ in the range $(0 < x \leq \Delta x)$ and $g(x) = 0$ in the range $(\Delta x < x \leq L)$.

This means that we are considering:

$$\begin{aligned} C_n^* &= \frac{2}{L\beta_n} \int_0^{\Delta x} \frac{100}{RC} \sin\left(\frac{n\pi x}{L}\right) \mathrm{d}x \\ &= \frac{-2}{n\pi\beta_n} \frac{100}{RC} \left[\cos\left(\frac{n\pi x}{L}\right)\right]_{x=0}^{x=\Delta x} \\ &= \frac{-200}{n\pi\beta_n RC} \left[\cos\left(\frac{n\pi\Delta x}{L}\right) - 1\right]. \end{aligned} \tag{27}$$

So, Eq. 22 reduces to:

$$V(x,t) = 100\left[\frac{L-x}{L}\right] + 100e^{-\frac{\Delta t}{2}} \sum_{n=1}^{\infty} \left[\frac{-200}{n\pi\beta_n RC}\left[\cos\left(\frac{n\pi\Delta x}{L}\right) - 1\right] \sin\beta_n t\right] \sin(k_n x). \tag{28}$$

The final step is to replace relevant parameters in Eq. 28 by their TLM equivalents.

5 The Spectral Radius of a TLM Scheme as a Function of τ

A numerical scheme for an elliptic PDE can be represented as [4, p. 235]:

$$\mathbf{A}x = 0 \tag{29}$$

where **A** is a large, sparse matrix. For many schemes this matrix partitions as:

$$\mathbf{A} = \mathbf{D} - \mathbf{L} - \mathbf{U} \tag{30}$$

and is the basis for many solution schemes. Using potential as the variable the discretised form of the scheme can be represented in a general way as [17]:

$$_{m+1}\mathbf{V} = \mathbf{M}\,_m\mathbf{V}. \tag{31}$$

The spectral radius of **M**, $\Re(M)$ is the largest eigenvalue of **M** and for a scheme to be stable the condition $\Re(M) < 1$ must apply. Many textbooks (e.g. Morton and Meyer [4, p. 235] use these principals to analyse the acceleration properties of the successive over-relaxation SOR finite difference scheme. Flaherty [17] gives a particularly clear presentation of this, where he demonstrates that a measure of the rate of convergence can be given by $-\ln[\Re(M_{\mathrm{SOR}})]$. At first sight TLM does not fit into this treatment because it is a two step scheme, but Flaherty's treatment of the duFort–Frankel scheme [18] provides the clue. We write the TLM algorithm as:

$$_{m+1}V(x) = \tau\left(_mV(x+1) + {}_mV(x-1)\right) + (1-2\tau)\,_{m-1}V(x). \tag{32}$$

In matrix terms this can be expressed as

$$ {}_{m+1}\boldsymbol{V} = \boldsymbol{A}\ {}_{m-1}\boldsymbol{V} + \boldsymbol{B}\ {}_{m}\boldsymbol{V}. \tag{33} $$

This is then rewritten as:

$$ \begin{bmatrix} {}_{m+1}\boldsymbol{V} \\ {}_{m}\boldsymbol{V} \end{bmatrix} = \begin{bmatrix} \boldsymbol{B} & \boldsymbol{A} \\ \boldsymbol{I} & \boldsymbol{0} \end{bmatrix} \begin{bmatrix} {}_{m}\boldsymbol{V} \\ {}_{m-1}\boldsymbol{V} \end{bmatrix}. \tag{34} $$

This can be written in a one-level scheme as:

$$ \boldsymbol{W}_{m+1} = \boldsymbol{L}_{\Delta}\boldsymbol{W}_{m+1} \text{ where } \boldsymbol{L}_{\Delta} = \begin{bmatrix} \boldsymbol{B} & \boldsymbol{A} \\ \boldsymbol{I} & \boldsymbol{0} \end{bmatrix}. \tag{35} $$

The spectral radius of this matrix as a function of acceleration parameter can be investigated numerically for different spatial discretisations. So, for a one-dimensional computational space with five nodes $\boldsymbol{L}_{\Delta}$ is a 10×10 matrix with:

$$ \boldsymbol{A} = \begin{bmatrix} 1-2\tau & 0 & 0 & . & . \\ 0 & 1-2\tau & 0 & . & . \\ 0 & 0 & 1-2\tau & . & . \\ . & . & . & . & 0 \\ . & . & . & 0 & 1-2\tau \end{bmatrix} \text{ and } \boldsymbol{B} = \begin{bmatrix} 0 & \tau & 0 & . & . \\ \tau & 0 & \tau & . & . \\ 0 & \tau & 0 & . & . \\ . & . & . & . & \tau \\ . & . & . & \tau & 0 \end{bmatrix}. \tag{36} $$

Inserting a value for τ we can calculate the maximum eigenvalue (the spectral radius).

6 Numerical Experiments and Observations

The objective in this section is to undertake TLM numerical calculations to make comparisons with other methods and to draw conclusions based on the similarities and differences in the results which are obtained.

In a previous paper de Cogan et al. [13] observed a small discrepancy between the optimum value of τ/ρ derived from TLM numerical simulations at different mesh sizes and that predicted from the transition from real to imaginary solutions in the Fourier analysis of a telegrapher's equation. As the present research developed it became apparent that some of the discrepancies which were reported in [13] when TLM results were compared with those from other methods might be due to subtle differences in the spatial location of the observation points of the different data sets. Conventional TLM is unusual in the way that we define interaction with the boundaries. This induces us to monitor the node points as shown in Fig. 7. In order

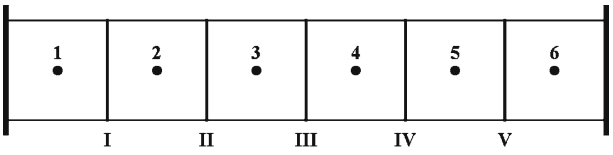

Fig. 7 A discretised space showing the points at the node centres which are monitored in a conventional TLM simulation. The problem space has six nodes, but it also has five inter-nodal zones

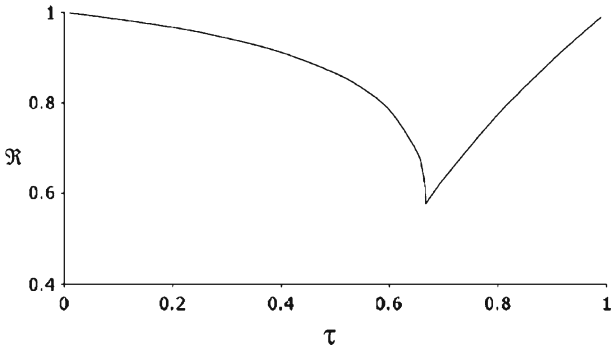

Fig. 8 Plot of the spectral radius for $M = 5$ as a function of τ for the underlying difference scheme that TLM represents

to have synchronism of arrival of pulses there is a distance Δx between node points, but a distance $\Delta x/2$ between a node point and a boundary. Although this can be accommodated in a Fourier solution, it is significantly more difficult in spectral radius and other calculations. The problem space in Fig. 7 has six nodes, but it will be seen that it has five inter-nodal zones. Published work on SOR as well as spectral radius calculations would interpret this as $M = 5$. This can in fact be accommodated using a hybrid form of TLM. In conventional TLM we have scattering at the node centres at discrete time intervals $m = 1, 2, 3, \ldots$ and during a time Δt pulses travel to adjacent nodes. However, at times $(m + 1/2)\Delta t$, just as ${}^sV_L(1)$ and ${}^sV_R(6)$ are interacting with their respective boundaries, so ${}^sV_R(1)$ and ${}^sV_L(2)$ are crossing zone I. We can define the potential at the zones as:

$$\Phi\,(I) = {}^sV_R\,(1) + {}^sV_L\,(2)\,. \tag{37}$$

The potentials at all other zones are similarly defined. This approach was used in all TLM simulations which are presented in the remainder of this paper and the results are very encouraging.

For purposes of comparison a plot of the spectral radius as a function of τ for the underlying difference scheme that TLM represents is shown in Fig. 8. It is immediately obvious that the shape is quite different, but the reasons for this lie in the exponential that is found in Eq. 28. No such factor is found in the spectral radius expressions, so that we can reduce the problem to a level playing field by plotting the natural logarithm of the number of iterations which are required to reach a required global error[4] limit against τ then the plots look much more alike—an example of this can be seen in Fig. 10b which is discussed later in this paper.

There was some indication in previous work [13] that the optimal value of τ/ρ for a given discretisation changed by a small amount if the global error criterion was altered. This conjecture was investigated in detail. It was found that optimal value of τ/ρ for a given discretisation did indeed reduce as the global error magnitude was reduced. This is shown in Table 2 for two different discretisations, where the equivalent optimum results derived from spectral radius estimates are also included. We see that for $M = 5$ the optimum spectral radius value of (τ/ρ) is 2 while the

[4]Global error $\varepsilon\,(k) = \sqrt{\frac{1}{M}\sum_{x=1}^{x=M}\left(\frac{V_{\text{analytical}}(x) - {}_mV_{\text{TLM}}(x)}{V_{\text{analytical}}(x)}\right)^2}$ (M is the number of nodes).

Table 2 Comparison of TLM and spectral radius optimum conditions for two discretisations at different levels of global error

M	$(\tau/\rho)_{\text{optimum}}$ TLM	Global error	$(\tau/\rho)_{\text{optimum}}$ spec. radius.
5	2.033	10^{-5}	
5	2.022	10^{-7}	
5	2.012	10^{-10}	
5			2.00
6	2.35	10^{-10}	
6	2.33	10^{-14}	
6			2.32

equivalent optimum TLM value for 10^{-10} global error is 2.012. For $M = 6$ the optimum spectral radius value of (τ/ρ) is 2.32 while the equivalent optimum TLM value for 10^{-14} global error is 2.33. These results would seem to suggest that the spectral radius optimal value is the same as our hybrid TLM value at infinitesimal error.

In developing a criterion based on the transition from the real to imaginary components in the Fourier solution of an equivalent PDE [13] we based our analysis on a unit velocity, $\Delta x/\Delta t = 1$. Based on our requirement to inhibit the lowest harmonic in the Fourier solution, this yielded a relationship between τ/ρ optimum and the mesh discretisation, M:

$$\frac{\tau}{\rho} = \frac{M}{\pi}. \tag{38}$$

In some recent work which is awaiting publication we have used a form of 'reverse-engineering' to obtain the underlying PDE for various difference schemes. Our treatment for the scheme for conventional TLM nodes is reproduced in Appendix, where we show that Eq. 32 is equivalent to:

$$\frac{\partial^2 V}{\partial x^2} = \frac{(2\boldsymbol{\tau} - 1)}{\boldsymbol{\tau}} \frac{\Delta t^2}{\Delta x^2} \frac{\partial^2 V}{\partial t^2} + \frac{2\,(1 - \boldsymbol{\tau})}{\boldsymbol{\tau}} \frac{\Delta t}{\Delta x^2} \frac{\partial V}{\partial t}. \tag{39}$$

So we have a telegrapher's equation where the velocity is:

$$v = \sqrt{\frac{\boldsymbol{\tau}}{(2\boldsymbol{\tau} - 1)}} \frac{\Delta x}{\Delta t} \tag{40}$$

and the diffusion constant is:

$$D = \frac{1}{2} \left(\frac{\tau}{1 - \tau} \right) \frac{\Delta x^2}{\Delta t}. \tag{41}$$

These can be applied to the optimum condition, $A = 2B_n$ (see Eq. 21). Using $A = v^2/D$ and $B = k_n v$ where $k_n = n\pi/L$ and $L = M\Delta x$ we get a quadratic:

$$\left[2 \left(\frac{n\pi}{M} \right)^2 - 1 \right] \boldsymbol{\tau}_{\text{opt}}^2 - \left[\left(\frac{n\pi}{M} \right)^2 - 2 \right] \boldsymbol{\tau}_{\text{opt}} - 1 = 0. \tag{42}$$

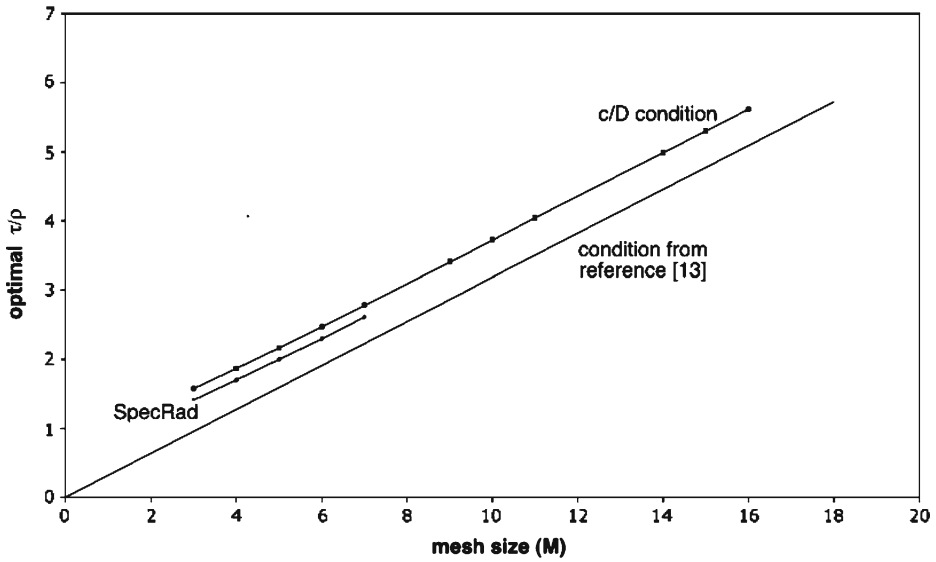

Fig. 9 Plots of optimum τ/ρ as a function of mesh discretisation (M is the number of inter-nodal zones). The line through the origin represents the relationship as derived in [13]. The points on the line annotated 'SpecRad' were derived from numerical evaluations of the optimum spectral radius. Points along the 'c/D' line were derived from Eq. 34 of this paper

The solutions for this equation as a function of M (with $n = 1$) are shown in Fig. 9 and it can be seen that all points over a large range of M (except perhaps at lowest values) lie along a straight line which is given by:

$$\left(\frac{\tau}{\rho}\right)_{\text{opt}} = 0.315M + 0.577. \tag{43}$$

The same figure also has results for spectral radius estimates of this parameter:

$$\left(\frac{\tau}{\rho}\right)_{\text{opt}} = 0.315M + 0.411. \tag{44}$$

The equivalent derived from Eq. 38 is of course:

$$\left(\frac{\tau}{\rho}\right)_{\text{opt}} = 0.318M. \tag{45}$$

So we now have a situation where we are at last comparing like with like, where the results of numerical simulations using our hybrid version of TLM are in very close agreement with spectral radius estimates when the global error limit is very small. We have moved from a situation of unit pulse velocity to one where the velocity varies as a function of τ. Our discrepancy has been much reduced, but it looks as if Eq. 40 might be a slight over-estimate. This could well be because Eq. 32 is still based on estimates at the conventional TLM nodal positions.

The next topic that needs to be addressed might be called the 'fine-structure' of convergence plots. If the numerical experiments are undertaken using very small intervals between successive values of τ we notice that the curves are not smooth,

but display 'wobbles'. There are a variety of reasons for this and a specific one is possibly due to the way in which convergence has been defined. Our programs have been designed to stop when the global error is less than some pre-set value. However, because time intervals are discrete it is possible that at time, $m\Delta t$ we may be above this criterion by an amount which may be large or small and at time $(m+1)\Delta t$ we may be below by an amount that is small or large. Figure 10a shows a result for hybrid TLM with $M = 5$. A detail of this is shown in Fig. 10b where it can be seen that the minimum point is not singularly defined. The two wobbles to the right of the minimum point(s) are due to the effects of discrete iteration steps. Figure 11a, b shows similar results for conventional TLM with $M = 6$ more fine structure. The two dips are almost same in both hybrid and conventional, and they are within the range of error difference between the two lines in Fig. 9 that do not go through the origin. However, we believe that there may be more to these results than simply a discrete iteration effect. If we simply record the global error as a function of iteration for different values of τ we also see oscillatory behaviour. The results of such calculations are plotted on a logarithmic scale for τ on either side of the optimum for the case of $M = 5$ and are shown in Fig. 12a, b. We note that for values less than optimum (the diffusion dominated region), we have no wobbles. Even at optimum we may have inhibited the Fourier $n = 1$ component in Eq. 28, but the $n = 2, 3, 4$ components may still play a role.

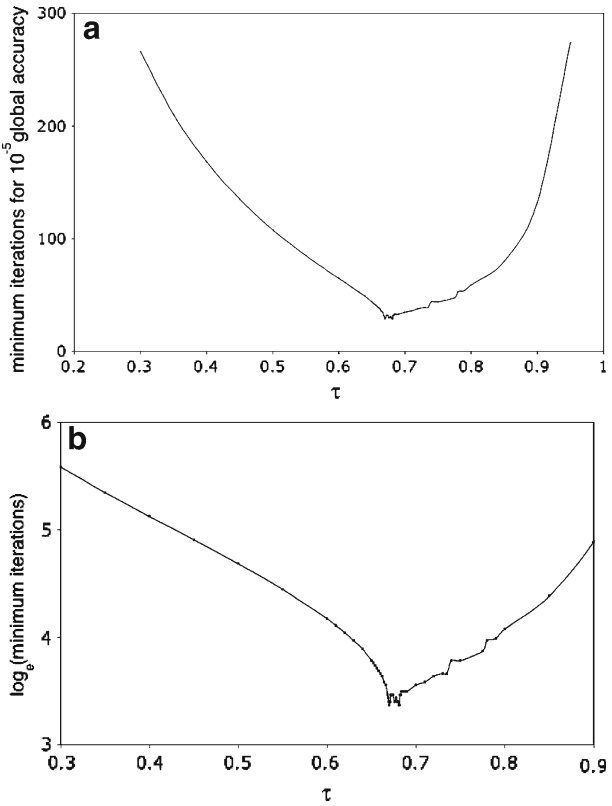

Fig. 10 **a** Plot of the minimum number of iterations which are required in a hybrid TLM mesh with $M = 5$ to achieve a global error less than 10^{-5} as a function of τ. **b** Detail of **a** in the vicinity of the optimum point plotted as the natural logarithm of the minimum number of iterations

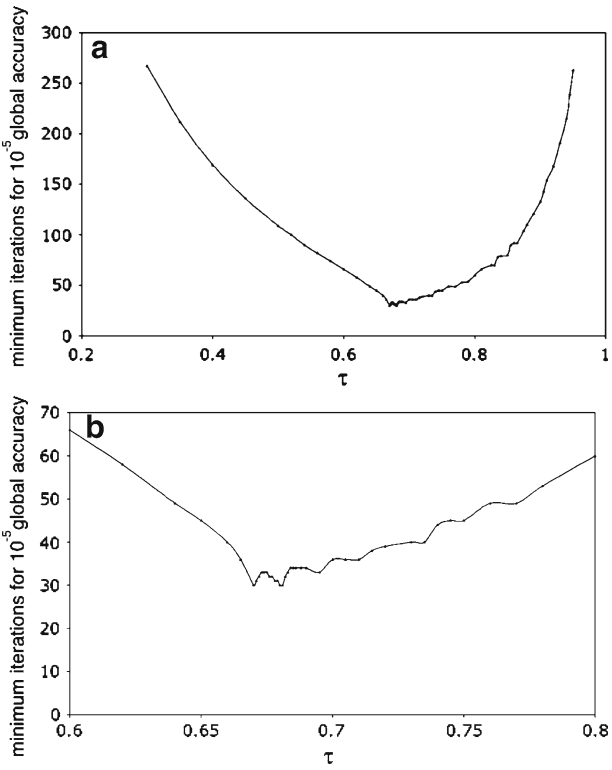

Fig. 11 **a** Plot of the minimum number of iterations which are required in a conventional TLM mesh with $M = 6$ to achieve a global error less than 10^{-5} as a function of τ. **b** Detail of **a** in the vicinity of the optimum point

Finally we come to a comparison between TLM numerical results and those obtained from a Fourier analysis of the same problem. Specifically, we consider the transient term of Eq. 28:

$$100e^{-\frac{\rho}{\tau}m}\sum_{n=1}^{\infty}\left[\frac{-200}{n\pi\beta_n\left(\frac{\rho}{\tau}\right)\Delta t}\left[\cos\left(\frac{n\pi}{M}\right)-1\right]\sin\beta_n m\Delta t\right]\sin\left(\frac{n\pi x}{M\Delta x}\right). \tag{46}$$

Initial results have not been as promising as we might have wished and we are forced to ask some questions. The first is concerned with the nature of convergence. What does it really mean when the global error is said to be less than a specified threshold? Given that we have harmonic contributions we can have a point, m in discrete time where the sum is indeed below the threshold while at iterations points, $m + 1$ or $m-1$ this does not occur. We can have a local convergence much earlier than is guaranteed by the enveloping exponential term. We must also ask whether we are comparing like with like. In the case of comparisons between TLM and spectral radius calculations this is now quite clear. In the case of TLM/Fourier comparisons, we can only say that we believe this to be the case, but we are still faced with some problems because of the definition of the critical term in Eq. 46:

$$\beta_n = \frac{\sqrt{4B_n^2 - A^2}}{2}, \tag{47a}$$

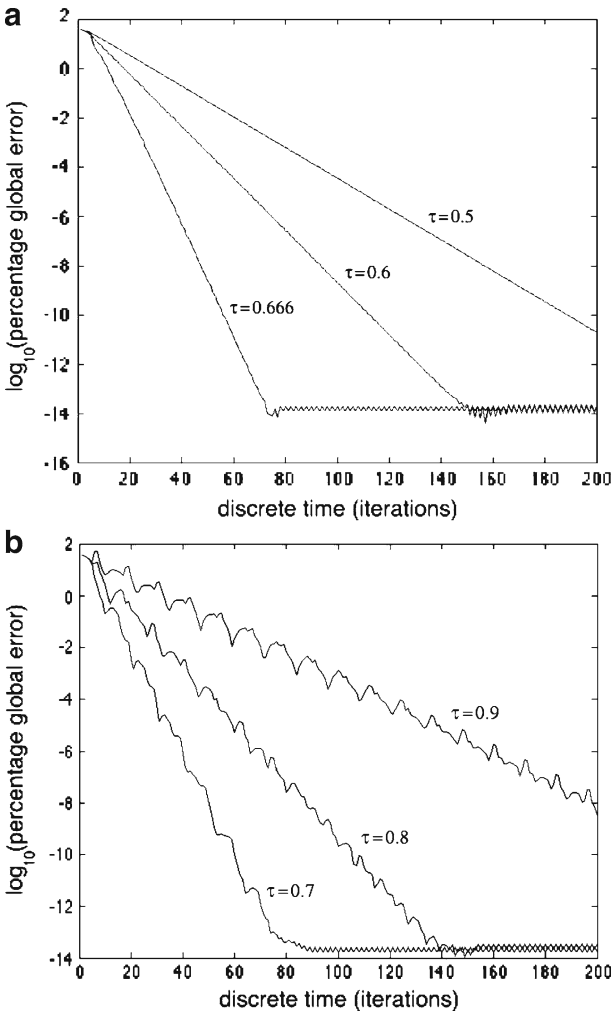

Fig. 12 Plots of $\log_{10}$ (global error) as a function of iteration time for τ on either side of the optimum value (spectral radius $\tau_{\text{optimum}} = 0.666$) for a five node conventional TLM simulation of the Laplace equation. **a** $\tau \leq \tau_{\text{optimum}}$, **b** $\tau > \tau_{\text{optimum}}$

$$\beta_n = \frac{\sqrt{\left(\frac{n\pi}{M}\right)^2 - \left(\frac{\rho}{\tau}\right)^2}}{\Delta t}. \tag{47b}$$

For τ values less than the optimal where the ρ/τ term in Eq. 47b dominates we would have to deal with imaginary quantities. In spite of these misgivings initial comparisons revealed that it was essential to replace a fixed value of velocity in $A = c^2/D$ by a τ dependent value as given in Eq. 40 (this of course then faces us with the problem that the velocity becomes infinite at $\tau = 0.5$). The $m(\tau)$ behaviour of the Fourier results then came much closer to the TLM result and it was found that if one used a normalisation factor, then close agreement could be obtained over a reasonable range of τ. This was achieved by noting the vertical shift needed to obtain agreement in the case of one point. In this case we considered the case where

TLM convergence required 75 iterations whereas the same value of τ used in Eq. 46 required 83 iterations to reach the same global error limit. All Fourier data points greater than τ_{opt} were multiplied by a factor 75/83 and the results are shown in Fig. 13. In the course of the numerical experiments associated with this figure we noted that unlike the case with TLM, changes in τ in the vicinity of the optimal value had very little effect on the outcome. Clearly $\sin(\beta_n k\Delta t)/\beta_1 \to m\Delta t$ as $\beta_1 \to 0$, so that the value of m is determined by the other harmonics. Nevertheless, there remains yet another point of disparity which can be seen in Fig. 13. The left-most point in the normalised Fourier results represents the case where $\beta_1 = 0$ and it is clearly displaced some distance from the TLM result. The match between Fourier and TLM values for τ_{opt} can be improved for an error limit of 10^{-5} if at $M = 5$ we change the value τ dependent velocity term A in Eq. 47a to $0.91A$. For the case of $M = 6$ the same agreement requires A to be multiplied by a factor $0.95A$. It is unlikely that these shifts can be due to the velocity term in $A = c^2/D$. Suspicion must therefore fall on the diffusion term. Our derivation both here and in [19] gives no hint of anything but a diffusion constant given by:

$$D = \frac{\Delta x^2}{2\Delta t}\,\frac{\tau}{\rho}. \tag{48}$$

However, studies of the variance in the 'Gaussian' profiles in TLM diffusion models excited by a single shot injection have highlighted a feature of TLM [19]. Whereas the variance in a conventional Gaussian diffusion can be reduced in TLM terms to:

$$\boldsymbol{\sigma}^2(k) = \frac{\boldsymbol{\tau}}{\boldsymbol{\rho}} m. \tag{49}$$

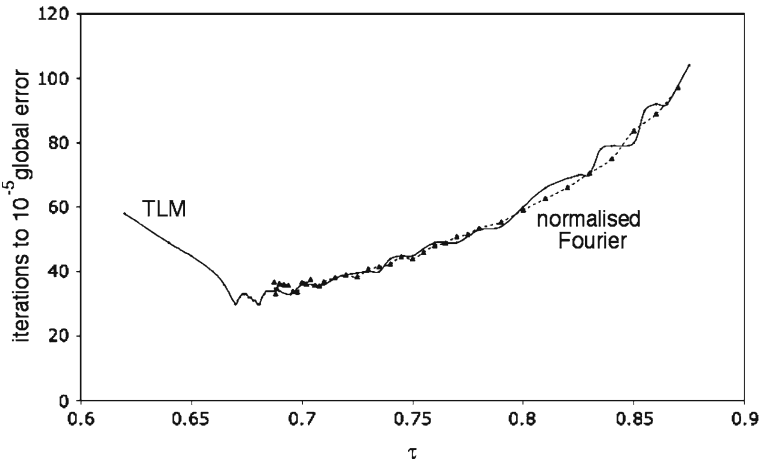

Fig. 13 Minimum iterations, m to achieve a global error below 10^{-5} as a function of τ for $M = 5$. The TLM results are shown as a *solid line*. The *dotted line* with triangle points represent the velocity dependent Fourier-derived values of k which have been 'normalised' (in order to superimpose the two plots each Fourier value of k has been multiplied by a factor 0.9375, i.e. 75/83)

TLM numerical experiments have shown that there are extra terms and an analytical treatment of the TLM scattering process has shown the variance is in fact:

$$\sigma^2(m) = \frac{\tau}{\rho}m - \frac{\tau-\rho}{2\rho^2} + \frac{(\tau-\rho)^{m+1}}{2\rho^2}. \tag{50}$$

We believe that the 'Diffusion' term in TLM is also contained in the spectral radius analysis, but has not so far been reflected in the Fourier treatment described here.

7 Conclusions

In this paper we have attempted to clarify the relationship between the scattering parameters in TLM algorithms for the Laplace equation and the rate of convergence to prescribed error limits. Mesh scaling has been used to provide a basis for the initial condition which minimises oscillatory behavior and we have been able to use this in an extension of previous work on developing an analytical solution to the same problem based on Fourier series. Numerical experiments based on small discretisations have shown a high degree of agreement between TLM results and those derived from matrix spectral radius calculations. The ensuing investigations on the relationship between the optimum scattering parameters and the mesh discretisation yield a slope which appears very close to $1/\pi$. They also confirm that it is essential in any analysis to consider a τ-dependent velocity.

Efforts to correlate TLM results with those derived from a Fourier analysis have proved much harder to achieve as there appears to be many facets to the problem. However, there is one aspect that might be significant and this came to light as we considered the apparent convergence of data points in Fig. 3. The limit line at the top of that figure appears to be heading towards a value of approximately 37 V as $S \to \infty$. While the points which start off at 50 V appear to be heading towards 18 V on a similar slope. In analysing this feature we attempted to use Eq. 32 to yield an algebraic expression for each of the sub-nodes at a given scaling. By this analysis it is easy to see that the initial excitation (50 V) propagates to the right according to Eq. 32 so that after S iterations, the value at the S-th node (the one next to the grounded boundary will be given by $50\tau^{S-1}$ and this agrees with the data in Table 1.

We know from Eq. 9b that $\rho = \frac{1}{1+S}$ and therefore $\tau = \frac{S}{1+S}$.

In the limit as $S \to \infty$ we have $\left[\frac{S}{1+S}\right]^{S-1} = e^{-1}$ so that 18.39 is to be expected.

The second node from the right-hand (grounded) boundary at any value S, does converge to $100e^{-1}$ but the path is slightly more subtle. This is because after the initial injection what is scattered to the left at the left-most node is 50ρ so that according to Eq. 10 what is incident at the next iteration is in fact $(100 - 50\rho)$. It is this that then propagates to the right and after S iterations the value at the $(S-1)$th node is $(100 - 50\rho)\tau^{S-2}$ or $\left(100 - \frac{50}{(1+S)}\right)\left(\frac{S}{1+S}\right)^{S-2}$ which agrees with the data in Table 1:

$$\text{As } S\to\infty\left(100 - \frac{50}{(1+S)}\right)\left(\frac{S}{1+S}\right)^{S-2} \to 100\left(\frac{S}{1+S}\right)^{S-2} = 100e^{-1} \text{ (i.e. 36.79 V)}.$$

After the second injection from the 100 V boundary a fraction $\rho(100 - 50\rho)$ is reflected back to the boundary. The next pulse incident from the boundary is therefore $100 - \rho(100 - 50\rho)$.

From these observations we can deduce that although very useful, Eq. 32 of itself cannot take account of the fact that the level of injection at the left-most (high value) boundary changes at every iteration and we must therefore assume that Eq. 39 similarly does not. The velocity term in Eq. 39 is determined only by the scaling. We conjecture that the change of injection level at every iteration implies an equivalent change in the transmission coefficient (and therefore velocity) across this boundary. This point clearly requires further investigation.

Acknowledgement The contribution of Lars Haartveit to the progression of this paper is noted. The authors would also like to express their gratitude to one of the referees for their very constructive comments which have been of significant benefit in the preparation of a revised manuscript.

Appendix: The PDE Which Underlies the TLM Algorithm

If we start with Eq. 32 we have:

$$_{m+1}V(x) = \tau\left[{}_mV(x+1) + {}_mV(x-1)\right] + (1-2\tau)\,{}_{m-1}V(x)$$

which can be written as:

$$_{m+1}V(x) = \tau\left[{}_mV(x+1) + {}_mV(x-1) - 2{}_mV(x)\right] + 2\tau\,{}_mV(x) + (1-2\tau)\,{}_{m-1}V(x).$$

Using the conventional finite difference approximations for second derivatives we have:

$$_{m+1}V(x) = \tau\Delta x^2\frac{\partial^2 V}{\partial x^2} + 2\tau\,{}_mV(x) + (1-2\tau)\,{}_{m-1}V(x)$$

$$_{m+1}V(x) = \tau\Delta x^2\frac{\partial^2 V}{\partial x^2} - {}_mV(x) + 2\tau\,{}_mV(x) + {}_mV(x) + (1-2\tau)\,{}_{m-1}V(x)$$

$$_{m+1}V(x) = \tau\Delta x^2\frac{\partial^2 V}{\partial x^2} + (2\tau-1)\,{}_mV(x) - (2\tau-1)\,{}_{m-1}V(x) + {}_mV(x)$$

$$_{m+1}V(x) + (2\tau-1)\,{}_{m-1}V(x) - (2\tau-1)\,{}_mV(x) = \tau\Delta x^2\frac{\partial^2 V}{\partial x^2} + {}_mV(x)$$

further additions and balances yields:

$$(2\tau-1)\frac{\partial^2 V}{\partial t^2}\Delta t^2 = \tau\frac{\partial^2 V}{\partial x^2}\Delta x^2 - 2(1-\tau)\frac{\partial V}{\partial t}\Delta t$$

so we end up with:

$$\frac{\partial^2 V}{\partial x^2} = \frac{(2\tau-1)}{\tau}\frac{\Delta t^2}{\Delta x^2}\frac{\partial^2 V}{\partial t^2} + \frac{2(1-\tau)}{\tau}\frac{\Delta t}{\Delta x^2}\frac{\partial V}{\partial t}$$

which is clearly a telegrapher's equation:

$$\frac{\partial^2 V}{\partial x^2} = \frac{1}{c^2}\frac{\partial^2 V}{\partial t^2} + \frac{1}{D}\frac{\partial V}{\partial t} \quad \text{where} \quad c = \frac{\Delta x}{\Delta t}\sqrt{\frac{\tau}{(2\tau-1)}} \text{ and } D = \frac{1}{2}\left(\frac{\tau}{\rho}\right)\frac{\Delta x^2}{\Delta t}.$$

References

1. Southwell, R.V.: Relaxation Methods in Engineering Science. Oxford University Press, Oxford, UK (1940)
2. Dusinberre, G.M.: Numerical Analysis of Heat Flow, pp. 121–125. McGraw-Hill, New York (1949)
3. Ames, W.F.: Numerical Methods for Partial Differential Equations. Academic, New York (1977)
4. Morton, K.W., Mayers, D.F.: Numerical Solution of Partial Differential Equations. Cambridge University Press, Cambridge, UK (2005)
5. Christopoulos, C.: The Transmission Line Modelling Method. IEEE, Piscataway, NJ (1995)
6. de Cogan, D.: Transmission Line Matrix (TLM) Techniques for Diffusion Applications. Gordon and Breach, Reading, UK (1998)
7. Smith, A.: Transmission line matrix modelling, optimisation and application to adsorption phenomena. B.Eng. thesis, Nottingham University (1988)
8. Al-Zeben, M.Y., Saleh, A.H.M., Al-Omar, M.A.: TLM modelling of diffusion, drift and recombination of charge carriers in semiconductors. Int. J. Numer. Model. **5**, 219–225 (1992)
9. de Cogan, D.: The relationship between parabolic and hyperbolic transmission line matrix models for heat-flow. Microelectron. J. **30**, 1093–1097 (1999)
10. Johns, P.B.: A simple, explicit and unconditionally stable routine for the solution of the diffusion equation. Int. J. Numer. Methods Eng. **11**, 1307–1328 (1977)
11. de Cogan, D.: Propagation analysis for thermal modelling. IEEE Trans. Compon. Packaging Manuf. Technol. Part A **21**, 418–423 (1998)
12. de Cogan, D., Chakrabarti, A., Harvey, R.W.: TLM algorithms for Laplace and Poisson fields in semiconductor transport. SPIE Proc. **2373**, 198–206 (1995)
13. de Cogan, D., O'Connor, W.J., Gui, X.: Accelerated convergence in TLM algorithms for the Laplace equation. Int. J. Numer. Methods Eng. **63**, 122–138 (2005)
14. Frankel, S.: Convergence rates of iterative treatments of partial differential equations. Math. Tables Other Aids Comput. **4**, 65–75 (1950)
15. de Cogan, D., O'Connor, W.J., Pulko, S.H.: Transmission Line Matrix (TLM) in Computational Mechanics (See Chapter 2 and 3). CRC, Boca Raton, FL (2006)
16. Gui, X., de Cogan, D.: Boundary conditions in TLM diffusion modeling. Int. J. Numer. Model. **19**, 69–82 (2006)
17. Flaherty, J.E.: Rensselaer polytechnic institute units CSCI-6840/MATH-6840 "partial differential equations" lecture 9. http://www.cs.rpi.edu/~flaherje/
18. Flaherty, J.E.: Rensselaer polytechnic institute units CSCI-6840/MATH-6840 "partial differential equations" lecture 4. http://www.cs.rpi.edu/~flaherje/
19. Chardaire, P., de Cogan, D.: Distribution in TLM models for diffusion (part I: one-dimensional treatment). Int. J. Numer. Model. **15**, 317–327 (2002)